Fiber Crimp Analysis by Fractal Dimension

Yoichiro Muraoka, Kjyohiro Inoue, Hisako Tagaya and Kazuo Nishizawa

Textile Research Journal 1995 65: 454
DOI: 10.1177/004051759506500804

Fiber Crimp Analysis by Fractal Dimension

YOICHIRO MURAOKA

Heian Jogakuin Junior College, Nampeidai, Takatsuki 569, Japan

KIYOHIRO INOUE

F & D Laboratory, Takarazuka, 665, Japan

HISAKO TAGAYA

Shiga University, Hiratsu, Otsu, 520, Japan

KAZUO NISHIZAWA

Laboratory of Interfacial Technique, Kita-ku, Kyoto, 603, Japan

ABSTRACT

A box-counting method for determining the fractal dimensions of crimped fibers is discussed in detail. Using nylon 6 crimped filament magnified figures, an application of the method is demonstrated where the box-counting dimension (D_B) of nylon 6 has a distribution of 1.00–1.65. Eight animal fibers, cotton, and two other synthetic crimped fibers are also characterized by D_B distributions of 1.00–1.32. Modified random Koch curves are used to simulate crimped fiber shapes and to examine the relationship between Hausdorff's dimension (D_H) and D_B.

Various kinds of materials classified as fibers are thin, thread-like, and flexible. A general definition of fibers pays attention to their shape, that is, the least aspect ratio of practical fibers is 100 [1]. Another important characteristic of fibers is their flexibility. Some are naturally crimped and others have artificial waves added to them. The randomness of the twisted fiber shapes is difficult to describe, but it is desirable to be able to express the complexity of fiber shapes numerically, like the aspect ratio.

Mandelbrot's concept of fractal geometry [7] is one of the most mathematically convenient when estimating irregular sets, because it is based on measures that are relatively easy to treat. The theory of fractal geometry has been applied to experimental studies of irregular sets, such as the carbon black profile [6], the stream line in *suminagashi* and marbling [4], and the Shimanto River watercourse [5].

Fractal geometry is characterized by self-similarity (both exact and statistical) and non-integral dimensions. We regard the images of single fibers as a random fractal set, a kind of statistically self-similar object. Roughly speaking, the fractal dimension is a criterion of the prominence of irregularities in a set.

When Mandelbrot defined fractal, he singled out Hausdorff's dimension, which is the most basic and important of the widely varied fractal dimensions in use today. Hausdorff's dimension is defined by covering and can be applied to any set [3].

To a subset F of n-dimensional Euclidean space R^n, suppose that any non-empty bounded set U of R^n exists with the diameter $|U|$:

$$|U| = \sup \{ d(x, y) : x, y \in U \} \quad . \qquad (1)$$

Let $\{ U_i \}$ be a countable collection of sets of, at most, diameter δ that covers F; $\{ U_i \}$ denotes a δ-cover of F. For any $\delta > 0$ and non-negative number s, we define

$$H_\delta^s(F) = \inf \Big(\sum_{i=1}^{\infty} |U_i|^s : 0 < |U_i| \le \delta, \; F \subset \bigcup_{i=1}^{\infty} U_i \Big) \quad . \qquad (2)$$

Then let the diameter δ approach a limit as $\delta \to 0$,

$$H^s(F) = \lim_{\delta \to 0} H_\delta^s(F) \quad , \qquad (3)$$

where $H^s(F)$ is the s-dimensional Hausdorff measure of F. This is a step function, and the limiting value is 0 or ∞. Then there is a unique, real number of $s = D_H$ at which $H^s(F)$ jumps from ∞ to 0,

$$D_H = \sup \{ s : H^s(F) = \infty \} = \inf \{ s : H^s(F) = 0 \} \quad , \qquad (4)$$

where D_H is a Hausdorff dimension of F, a kind of covering dimension [2].

The advantages of D_H are mathematical strictness and clarity; moreover, it can include a nonintegral dimension different from a topological (Euclidean) dimension. If the varied complexity of the fractal patterns corresponds with D_H values in a unique way, it would be convenient for us to evaluate the complexity numerically. On the other hand, the major disadvantages are that it is hard to estimate by computational methods, it is ambiguous in finding the most efficient covering condition, and it is troublesome to take a limit.

Accordingly, D_H has no practical use, and many nonintegral covering practical dimensions have been advocated for Mandelbrot's fractal dimension. It involves three special dimensions: the similarity dimension (D_S), the compass (divider) dimension, and the box-counting dimension D_B [8]. These are easy to treat and equivalent to D_H under suitable conditions. Of the three, we have chosen D_B to describe the complexity of the fibers. Since there are five equivalently defined ways of finding D_B [2], we take the number of d-mesh cubes that cover the set. We estimate the D_B of the crimped single fibers and simulate their shapes using a modified random Koch curve recursive graphic program.

Experimental

MATERIALS

Crimped single fibers examined in this study are summarized in Table I. Animal fibers were supplied by Fukaki Woolen Textile Co. (Izumi-otsu, Osaka, Japan). Egyptian (Sea Island) cotton batting and two-dimensional regular crimped polyester staple processed by the stuffer box method, Toray Tetoron, were supplied by Kikuya Co. (Otsu, Japan). Both are mixed and used as stuffing materials for Japanese mattresses or futons.

Acrylic fiber, Exlan K8VC, with crimps added by the stuffer box method and then cut into variable lengths, was supplied by Toyobo Co. (Osaka, Japan). It is used in blending with wool. Nylon 6 crimped filament yarn, Toray Avilas [110/2-24F], made by the false-twist process and used for hosiery, was supplied by Okamoto Co. (Koryo-cho, Nara, Japan).

One hundred specimens were measured for each fiber. These specimens were carefully pulled out from loose fibers without applying tension, then copied as they were. We discarded the fibers suffering initial tension because tension decreased the dimension.

TABLE I. Fibers used in this study.

Sample code	Fiber	Length, mm	Diameter, μm
A	alpaca	190	20–65
B	angora rabbit	52–132	14–50
C	camel	30–130	12–48
D	cashmere goat	30–80	5–19
E	guanaco	20–90	10–35
F	merino sheep (wool)	85–170	11–26
G	mohair (angora goat)	46–187	18–58
H	vicuna	20–70	9–28
I	cotton	16–40	1–6
J	polyester	64	27 ($7d^a$)
K	acrylic	60–120	19 ($3d^a$)
L	nylon 6	–	24 ($4.6d^a$)

[a] d = denier.

BOX-COUNTING DIMENSION D_B

We put the copied fiber image onto a regular grid of mesh size d and counted the number of grid boxes $N(d)$ that covered the image. We then used the same procedure to get corresponding numbers at different side lengths d of squares. There is a proportional relation between $N(d)$ and d^{-s} [2]:

$$N(d) \approx c d^{-s} \quad . \tag{5}$$

We might say that the set has a dimension s, and s is regarded as D_B. Taking logarithms, we get

$$\log N(d) \approx \log c - D_B \log d \quad . \tag{6}$$

Equation 6 is then rewritten to solve for D_B, and the term $\log c / \log d$ approaches 0 as $d \to 0$. This results in the following definition:

$$D_B = \lim_{d \to 0} \frac{\log N(d)}{-\log d} \quad . \tag{7}$$

Here, linearities are maintained within a finite range of d for Equation 6, and so D_B is estimated by the slope of a log-log graph plotted regression line over a suitable range of d without taking a limit.

MODIFIED RANDOM KOCH CURVE AND ITS SIMILARITY DIMENSION D_S

We used modified random Koch curves to simulate the shapes of the crimped single fibers. Let a straight line segment of length L be the initiator (step 0) presented in Figure 1A. Then decide the summit point s such that the triangles EFS and GHS become isosceles triangles. The equilateral length a and s are fixed by the magnitude of the base angle θ (Figure 1B takes $\theta = 20°$). Replace L with a broken line of four segments having the same length a to make the generator (step 1). Repeating this procedure, we get a prefractal figure known as the modified Koch curve.

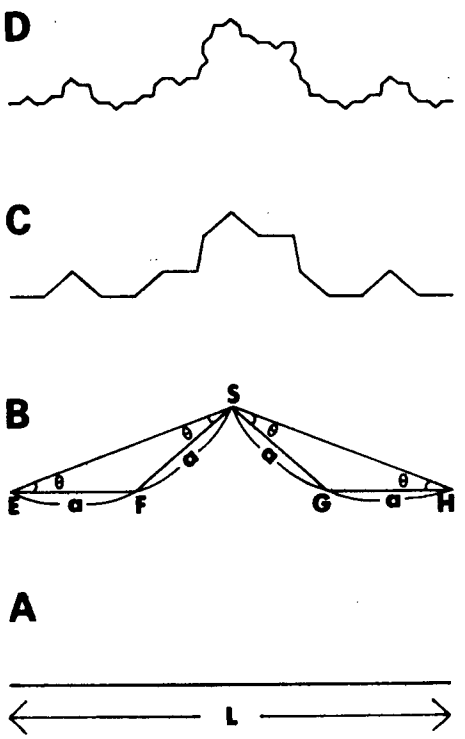

FIGURE 1. Construction of the modified random Koch curve: (A) initiator (step 0), straight line segment of length L, (B) generator (step 1) constructed by four same length a subsegments, θ (base angle) = 20°, (C) step 2 prefractal, θ = 20°, (D) step 3 prefractal, θ = 20°.

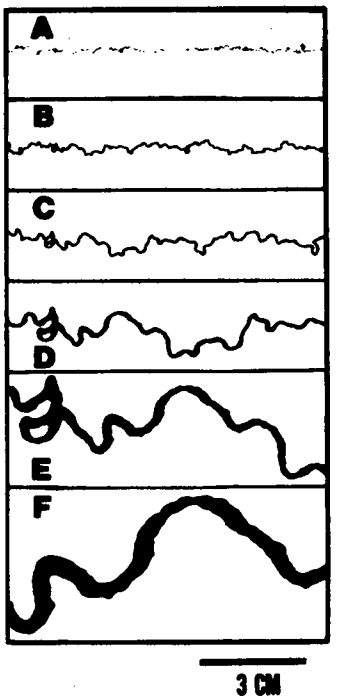

FIGURE 2. Magnified figures of nylon 6 crimped filaments: magnification factor A = 1, B = 2, C = 4, D = 8, E = 16, F = 32.

There are two possible orientations in the replacement step however. The baseless isosceles triangle at the middle part of the segment (FGS in Figure 1B) may go either to the convex or the concave. We determined the new orientation at random followed by a random number generator in each replacement step, which then yielded the modified random Koch curve. Examples are shown in Figures 1C (step 2) and 1D (step 3). The D_S value of the modified random Koch curve is given by

$$D_S = \frac{\log N}{\log (1/r)} \quad . \tag{8}$$

Here N is the number of subsegments scaled down by the reduction factor of r from its parent. The reduction factor r is obtained by

$$r = a/L \quad \left(a < \frac{1}{2}L\right) \quad . \tag{9}$$

Results and Discussion

MEASUREMENT CONDITIONS FOR BOX-COUNTING DIMENSION D_B

We obtained the magnified images from a 27 cm length of nylon 6 crimped filament by similarity transformation from a photocopier. The five copies were prepared using a magnification factor of 2–32 as compared to the original, which is partially shown in Figure 2. Each figure was cut to a length of 27 cm and put onto a d-mesh regular grid, an example of which is depicted in Figure 3. We counted the number of grid boxes $N(d)$ that intersect the figure. The side lengths of grid d were taken from 4 to 40 mm at intervals of 4 mm. These conditions took into account that the lower and upper limits d_{min} and d_{max} for d should span one decade of length or more in order for Equation 6

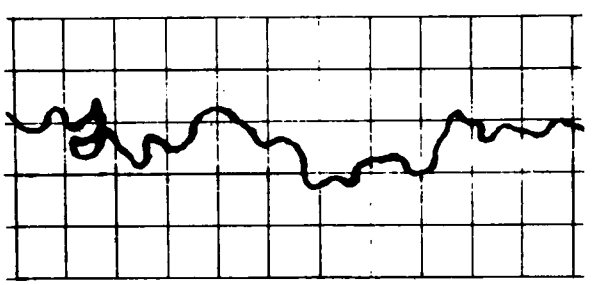

FIGURE 3. Part of the magnified figure of nylon 6 crimped filament that intersects the regular grid: magnification factor = 8, side length of grid = 8 mm.

to work [10]. A minimal condition is that d_{max}/d_{min} must exceed $2^{1/D}$ [9]. In the case of compass dimension, the step size should be smaller than 0.3 lengths of the figure [6]. The results are given in Table II. For each of the figures, we estimated D_B as the slope of the log-log graph plotted regression line in Equation 6. These results are shown in the second row from the bottom of Table II.

TABLE II. Number of grid boxes $N(d)$ to each side length d and box-counting dimensions D_B of nylon 6 crimped filament (values in parentheses were evaluated logarithmically).

Side lengths of grid boxes, cm	Magnification factor					
	1	2	4	8	16	32
0.4	68	78	87	104	122	110
(−0.916)	(4.220)	(4.357)	(4.466)	(4.644)	(4.804)	(4.700)
0.8	34	34	37	51	57	54
(−0.223)	(3.526)	(3.526)	(3.611)	(3.932)	(4.043)	(3.989)
1.2	23	23	23	31	35	36
(0.182)	(3.135)	(3.135)	(3.135)	(3.434)	(3.555)	(3.584)
1.6	17	17	17	21	24	29
(0.470)	(2.833)	(2.833)	(2.833)	(3.045)	(3.178)	(3.367)
2.0	14	14	14	16	22	22
(0.693)	(2.639)	(2.639)	(2.639)	(2.773)	(3.091)	(3.091)
2.4	12	12	12	12	15	16
(0.875)	(2.485)	(2.485)	(2.485)	(2.485)	(2.708)	(2.773)
2.8	10	10	10	10	12	15
(1.030)	(2.303)	(2.303)	(2.303)	(2.303)	(2.485)	(2.708)
3.2	9	9	9	9	9	13
(1.163)	(2.200)	(2.200)	(2.200)	(2.200)	(2.200)	(2.565)
3.6	8	8	8	8	8	12
(1.281)	(2.079)	(2.079)	(2.079)	(2.079)	(2.079)	(2.485)
4.0	7	7	7	7	7	10
(1.386)	(1.946)	(1.946)	(1.946)	(1.946)	(1.946)	(2.303)
D_B:d = 0.4~4.0 cm	0.957	1.018	1.066	1.204	1.251	1.034
D_B:d = 0.8~2.8 cm	-	0.966	1.022	1.310	1.205	-

Agreement of the regression line with the plotted data from the original size figure is so satisfactory over almost the entire range of d, as illustrated in Figure 4, that the lengths from 4 to 40 mm may be considered as suitable sides of grids for $N(d)$ estimation. The D_B value, however, is below unity. We proved that a set with $D_H < 1$ is totally disconnected [2]. Usually D_B is larger than D_H for a statistically self-similar set. Therefore, the systems that yield $D_B < 1$ are inappropriate methods for analyzing the crimps. The curve of the 32× magnified image is so smooth and thick that the crimps appear to vanish. This causes the small value of D_B to be nearly dimensionally equal to a straight line segment. Since these systems were not suitable for D_B estimation to describe the irregularities of the fiber shapes, we omitted them.

On the other hand, the D_B value was over unity for the 8 × magnified image, but the plotted data deviated from the regression line in places, *i.e.*, d = 4, 32, 36,

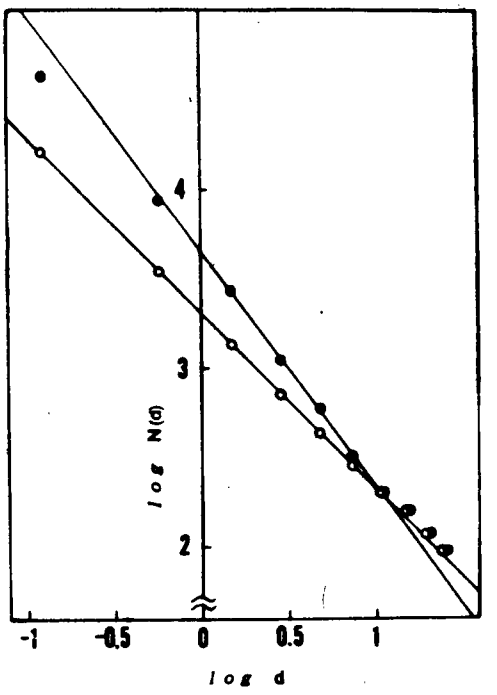

FIGURE 4. Double logarithmic diagram for estimating the box-counting dimensions of nylon 6. $N(d)$ = number of grid boxes, d = side lengths of grid in cm. ○ = original size figure, ● = 8 × magnified figure.

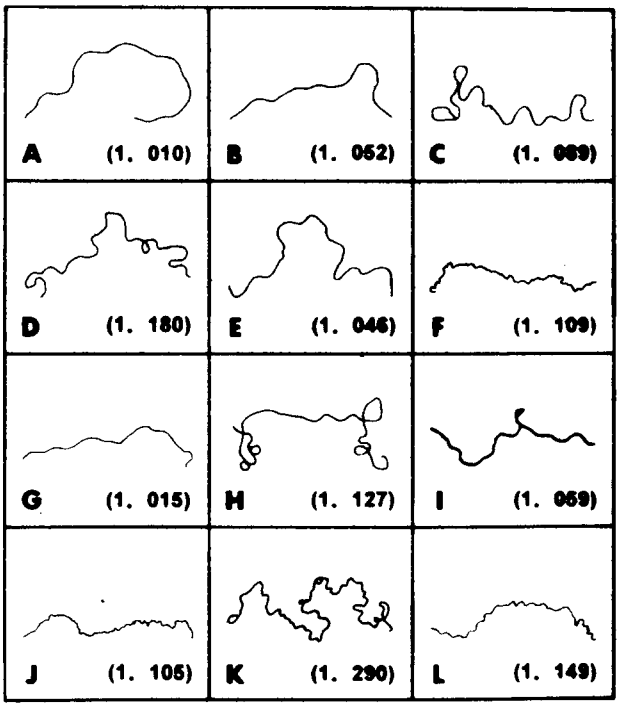

FIGURE 5. Sample figures of the crimped fibers: (A) alpaca, (B) angora rabbit, (C) camel, (D) cashmere goat, (E) guanaco, (F) merino sheep, (G) mohair, (H) vicuna, (I) Egyptian cotton, (J) acrylic, (K) nylon 6, (L) polyester. Values in parentheses are the box-counting dimensions.

and 40 mm, as depicted in Figure 4. Therefore, the D_B values were recalculated in the range of $d = 4 - 28$ mm for $2 - 16 \times$ magnified images. The results are given in the bottom row of Table II. The $8 \times$ magnified image, $4 - 28$ mm lengths of d system, showed the largest D_B value. As a matter of fact, there is no established theory about the magnification factor of a photocopy, but it is desirable when examining magnified crimp images. We chose the system above because the complexity of the copied fiber image was clearly detailed and the number of grid boxes was easy to count. We obtained D_B values that follow under these conditions.

Box-Counting Dimension Distribution of Crimped Fibers

Figure 5 shows samples of the figures copied from the crimped fibers. Values in parentheses are D_B; they increased with the increase in fiber twisting from 1.010 to 1.290. Accordingly, almost all the single fiber shapes extended from $D_B \doteqdot 1$ smooth curve to $D_B \doteqdot 1.3$ finely crimped wild structure inclusive.

In Figure 5, both F and J have almost the same D_B values despite the different images. It is only natural that differently crimped fibers have the same or extremely close D_B. Since there are global fractals and local fractals in a random fractal set [6], we took only average D_B values, so these values do not express detailed fractal dimensions corresponding uniquely to crimps. In characterizing fiber crimps, this method has a limitation. It is an imperfect way to estimate fiber crimps, and so another complementary parameter must be introduced to refine the method.

A characteristic of these fiber shapes is the fact that they always contain a wide distribution of D_B. The histograms of D_B distribution are summarized in Figure 6. Alpaca has both hair and wool features, so the loose

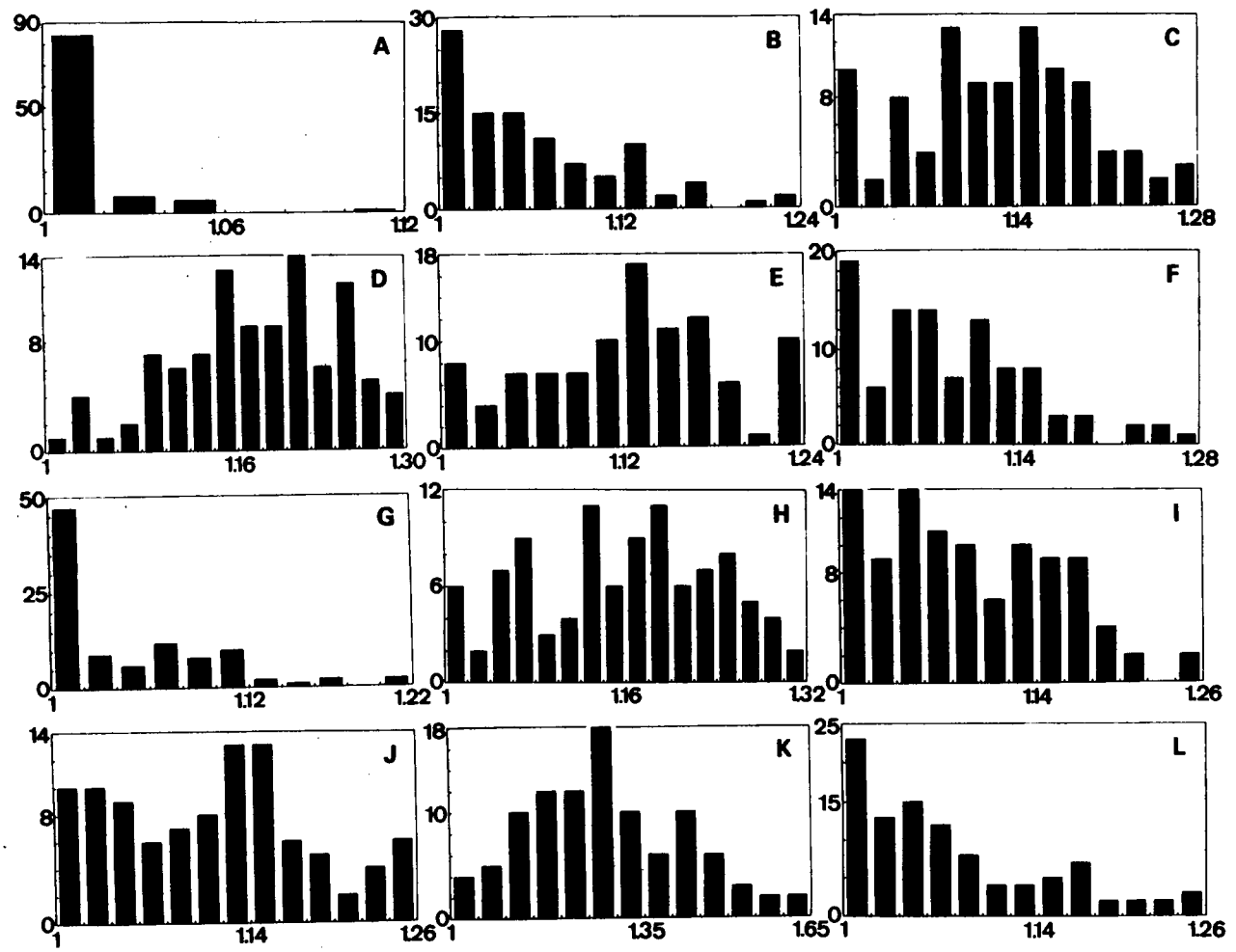

FIGURE 6. Box-counting dimension distribution of the crimped fibers. Ordinate: frequency, abscissa: box-counting dimension. (A) alpaca, (B) angora rabbit, (C) camel, (D) cashmere goat, (E) guanaco, (F) merino sheep, (G) mohair, (H) vicuna, (I) Egyptian cotton, (J) acrylic, (K) nylon 6, (L) polyester.

fiber specimen is a blend of coarse and fine fibers, resulting in nearly smooth curved figures of $D_B \doteqdot 1$. Mohair and angora have similar tendencies, but their shapes are somewhat complex. Camel, cashmere goat, guanaco, merino sheep, vicuna, and Egyptian cotton are fine loose fibers. Merino sheep and Egyptian cotton contain relatively large numbers of smooth curved fibers, and the D_B values decrease gradually from 1.00 to around 1.26. Guanaco and camel show a varied distribution; in particular, they contain many fibers between 1.08 to 1.20. Cashmere and vicuna are the most complicated animal fibers, many having D_B values over 1.20.

Since acrylic shows the maximum frequency at $D_B = 1.12 - 1.16$, it is suitable for blending with fine animal fibers such as cashmere and vicuna from the dimensional viewpoint. However, it contains comparatively numerous smooth curved fibers, the distribution being similar to that of merino sheep. We can understand why acrylic is supplied as a blend material for wool and other fine animal fibers. Egyptian cotton and polyester also have analogous distributions. Polyester's D_B value frequency gradually decreases from 1.00 to 1.26. After mixing, these fibers are used for futons. We obtained the nylon 6 distribution from the figures of cut single filaments pulled out from the crimped filament yarn. The single filaments have many fine crimps that resemble the shape of silk filaments just after being unwound from silkworm cocoons. They produced the extraordinarily wide distribution from 1.00 to 1.65. The modified random Koch curves have $D_S = 1.625$ at $\theta = 40°$, and the upper limit of the base angle of the curves is $\theta = 45°$, at which angle D_S reaches 2, a surface object.

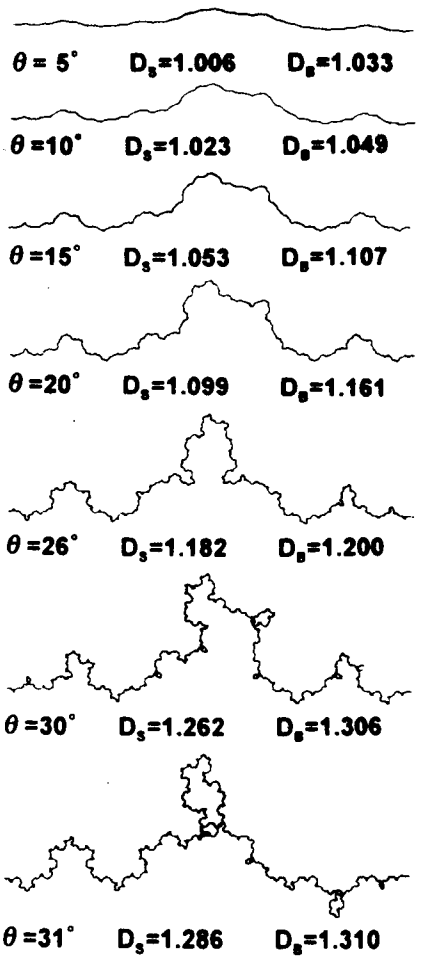

FIGURE 7. Examples of modified random Koch curves (step 5) used to simulate crimped fiber shapes. θ = base angle, D_S = similarity dimension, D_B = box-counting dimension.

BOX-COUNTING DIMENSION OF MODIFIED RANDOM KOCH CURVES

Figure 7 shows examples of modified random Koch curves chosen from the many computer graphics figures to simulate crimped fiber shapes. All of them are step 5 prefractal figures, and they adequately simulate the crimped fibers in the $\theta = 5°$ to $31°$ region.

For an exact self-similar set, the three fractal dimensions D_H, D_S, and D_B exactly achieve equality—$D_H = D_S = D_B$. But any statistical self-similar set has, in general, a larger D_B than D_H and D_S [2], so $D_H = D_S < D_B$. It is unclear how large D_B is, however, since we have little information about the relationship between D_H and D_B. Figure 7 compares D_S and D_B numerically. Within the range of these θ, D_B values are larger than D_S values to the extent of 0.018–0.062. Because D_S values increase steeply, accompanied by the increase of θ, this relationship was broken at the high θ region. For example, the D_B value was 1.390 at $\theta = 40°$. Simulations at base angles above 35° failed because the resemblance between fiber shapes and computer graphics figures deteriorated.

Our aim in this work is to disclose the relationship between fiber crimp and the mechanical characteristics of fiber lumps. So far, there have been few studies of fiber lump properties such as compressibility, resilience, elasticity, and softness relevant to the numerical values of fiber shapes. This is merely a preliminary report to estimate manually the complexity of single fiber shapes, but we believe that the box-counting measurement is one way to analyze fiber crimp and the first step toward crimp quantification.

We are currently examining a box-counting method that uses a computer image analyzing system, and we are inquiring into the relationship between single fiber

shapes and fiber mass properties. As a matter of course, the box-counting method has a limitation in characterizing fiber crimp, so it is necessary to investigate another complementary parameter. Nevertheless, refinement of this method may be useful for developing a new technique for fiber processing.

Literature Cited

1. Billmeyer, F. W., Jr., "Textbook of Polymer Science," 3rd ed., John Wiley & Sons, NY, 1984, p. 486.
2. Falconer, K., "Fractal Geometry," John Wiley & Sons, NY, 1990, pp. 25–53.
3. Hausdorff, F., Dimension and äusseres Mass, *Math. Ann.* **79,** 157–179 (1919).
4. Ishii, T., and Muro, J., The Fractal Aspect of Suminagashi and Marbling, *Thin Solid Films* **178,** 109–113 (1989).
5. Ishimura, S., and Ishimura, S., "Fractal Mathematics" (in Japanese), Tokyo Tosho, Tokyo, 1990, pp. 252–254.
6. Kaye, B. H., Image Analysis Techniques for Characterizing Fractal Structures, in "The Fractal Approach to Heterogeneous Chemistry: Surface, Colloids, Polymers," D. Avnir, Ed., John Wiley & Sons, NY, 1989, pp. 55–66.
7. Mandelbrot, B. B., The Fractal Geometry of Nature, W. H. Freeman & Co., NY, 1983.
8. Peitogen, H.-O., Jürgens, H., and Saupe, D., "Fractals for the Classroom, Part One," Springer-Verlag, NY, 1992, pp. 209–253.
9. Pfeifer, P., Fractal Dimension as a Working Tool for Surface-Roughness Problems, *Appl. Surf. Sci.* **18,** 146–164 (1984).
10. Pfeifer, P., and Obert, M., Fractals: Basic Concepts and Terminology, in "The Fractal Approach to Heterogeneous Chemistry: Surface, Colloids, Polymers," D. Avnir, Ed., John Wiley & Sons, NY, 1989, pp. 11–43.

Manuscript received June 21, 1994; accepted October 10, 1994